Atmos. Chem. Phys. Discuss., 12, 24735–24764, 2012
www.atmos-chem-phys-discuss.net/12/24735/2012/
doi:10.5194/acpd-12-24735-2012

Atmospheric Chemistry and Physics Discussions

The link between organic aerosol mass loading and degree of oxygenation: an α-pinene photooxidation study

L. Pfaffenberger, P. Barmet, J. G. Slowik, A. P. Praplan, J. Dommen, A. S. H. Prévôt, and U. Baltensperger

Laboratory of Atmospheric Chemistry, Paul Scherrer Institute, 5232 Villigen, Switzerland

Received: 23 July 2012 – Accepted: 31 August 2012 – Published: 20 September 2012

Correspondence to: A. S. H. Prévôt (andre.prevot@psi.ch)

Published by Copernicus Publications on behalf of the European Geosciences Union.

Abstract

A series of smog chamber (SC) experiments was conducted to identify driving factors responsible for the discrepancy between ambient and SC aerosol degree of oxygenation. An Aerodyne high resolution time-of-flight aerosol mass spectrometer is used to compare mass spectra from α-pinene photooxidation with ambient aerosol. Composition is compared in terms of the fraction of organic mass measured at *m/z* 44 (f_{44}), a surrogate for carboxylic/organic acids as well as the atomic oxygen-to-carbon ratio (O : C), vs. f_{43}, a surrogate for aldehydes, alcohols and ketones. Low (near-ambient) organic mass concentrations were found to be necessary to obtain oxygenation levels similar to those of low-volatility oxygenated organic aerosol (LV-OOA) commonly identified in ambient measurements. The effects of organic mass loading and OH (hydroxyl radical) exposure were decoupled by inter-experiment comparisons at the same integrated OH concentration. On average, an OH exposure of $2.9 \pm 1.3 \times 10^7\,\mathrm{cm^{-3}\,h}$ is needed to increase f_{44} by 1 % during aerosol aging. For the first time, LV-OOA-like aerosol from the abundant biogenic precursor α-pinene was produced in a smog chamber by oxidation at typical atmospheric OH concentrations. Significant correlation between measured secondary organic aerosol (SOA) and reference LV-OOA mass spectra is shown by Pearson's R^2 values larger than 0.90 for experiments with low organic mass concentrations between 1.5 and $15\,\mu\mathrm{g\,m^{-3}}$ at an OH exposure of $4 \times 10^7\,\mathrm{cm^{-3}\,h}$, corresponding to about two days oxidation time in the atmosphere, based on a global mean OH concentration of $\sim 1 \times 10^6\,\mathrm{cm^{-3}}$. Not only is the α-pinene SOA more oxygenated at low organic mass loadings, but the functional dependence of oxygenation on mass loading is enhanced at atmospherically-relevant precursor concentrations. Since the degree of oxygenation influences the chemical, volatility and hygroscopic properties of ambient aerosol, smog chamber studies must be performed at near-ambient concentrations to accurately simulate ambient aerosol properties.

ACPD

12, 24735–24764, 2012

1 Introduction

Organic aerosol (OA) represents 20 to 90 % of submicron atmospheric aerosol (Jimenez et al., 2009 and references therein) and has numerous sources. It can be introduced directly by combustion and mechanical processes into the atmosphere as primary organic aerosol (POA) or can be formed by condensation of gas phase reaction products with low vapor pressures resulting in secondary organic aerosol (SOA). Modeling of SOA formation and aging processes requires accurate prediction of both SOA mass concentration and composition. While traditional models underestimated the SOA burden (Volkamer et al., 2006), prediction of SOA mass has recently been improved through the use of the volatility basis set framework (Donahue et al., 2006; Robinson et al., 2007) although the system remains significantly underdetermined (Hodzic et al., 2010). In contrast, efforts to reproduce ambient SOA oxygenation levels using atmospherically-relevant OH concentrations have been largely unsuccessful. Here we explore the factors governing the degree of oxygenation of α-pinene SOA produced in smog chamber experiments.

Analysis of aerosol mass spectrometer (AMS) data using the source apportionment method positive matrix factorization (PMF) allows the total OA to be represented as a linear combination of factors representing various sources and/or processes. The SOA fraction is often represented in terms of semi-volatile oxygenated OA (SV-OOA) and low-volatility oxygenated OA (LV-OOA) (Lanz et al., 2007; Ulbrich et al., 2009; Jimenez et al., 2009). In addition to their volatility difference, SV-OOA has a lower atomic O : C ratio than LV-OOA and often represents fresh aerosol closer to the source, while LV-OOA, with a higher O : C ratio represents more aged OA (Ng et al., 2010; DeCarlo et al., 2010; Lanz et al., 2010).

Two AMS mass fragments previously shown to be useful in describing atmospheric SOA occur at *m/z* 44 (CO_2^+) and *m/z* 43 (mostly $C_2H_3O^+$ for SOA, with a lesser contribution from $C_3H_7^+$). The f_{44} value, being the ratio of the organic fraction of *m/z* 44 to total organics, has been empirically related to the atomic O : C ratio and is to a large part

ACPD
12, 24735–24764, 2012

derived from organic acids, of which a larger fraction is found in more aged aerosols (Aiken et al., 2008; Duplissy et al., 2011). The ratio of organic *m/z* 43 to total organics (f_{43}) is more closely related to fragmentation of aldehydes, ketones and alcohols. Taken together, f_{44} and f_{43} have been used to describe the set of LV-OOA and SV-OOA factors obtained by PMF analysis of 43 ambient datasets (Ng et al., 2010). SOA produced in smog chamber (SC) studies typically falls within the range of ambient SV-OOA, almost always showing lower degrees of oxygenation than ambient LV-OOA (Ng et al., 2010). These mass spectral differences suggest that SC SOA evaporates at lower temperatures than ambient LV-OOA. Although volatility is not directly measured in most studies, Huffman et al. (2009) show that SC SOA is typically more volatile than ambient SOA.

Not only volatility, but also hygroscopicity has been related to the organic mass fraction f_{44} and the atomic O : C ratio (Duplissy et al., 2008, 2011). More oxygenated particles take up more water at a given relative humidity, suggesting increased cloud formation potential. Measurements of dark α-pinene ozonolysis in a continuous flow chamber by Shilling et al. (2009) demonstrated that the aerosol chemical composition depends on the total organic mass concentration, however the generated aerosol was less oxygenated than ambient LV-OOA. Recently, LV-OOA-like aerosol was obtained in a smog chamber, but only by starting with oxygenated gas phase precursors (Chhabra et al., 2011), whereas most primary volatile organic compound emissions are thought to be more hydrocarbon-like. However, these results indicate that the location of SOA in the f_{44} to f_{43} space is affected by precursor identity.

Two recent studies performed in flow reactors did find SOA from α-pinene photooxidation that falls in the range of LV-OOA (Massoli et al., 2010; Lambe et al., 2011). The high OH concentrations (e.g. 2×10^9 to 2×10^{10} cm^{-3} in Lambe et al., 2011) produced in the flow reactors change the relative probabilities that a low-volatility reaction product collides with a particle and condenses as SOA or collides with an OH radical and reacts further, potentially remaining in the gas phase. Thus, the rapidly occurring chemistry may lead to a different set of products while inhibiting slower condensed phase reactions. Therefore the importance of heterogeneous reactions may also be

ACPD
12, 24735–24764, 2012

enhanced; Slowik et al. (2012) suggest that heterogeneous reactions at OH exposures of 3×10^8 cm^{-3} h are sufficient to transform the aerosol to LV-OOA-like composition.

The inability of smog chambers to generate α-pinene SOA with oxygenation, volatility and (potentially) hygroscopicity similar to ambient LV-OOA indicates an important gap in the current understanding of SOA production and aging. In this paper, an atmospherically relevant precursor for SOA, α-pinene, is selected. The aim of this study is to find the main driving factors responsible for the incapacity of smog chamber studies to yield LV-OOA-like aerosol from the biogenic precursor α-pinene, even in the limit of extensive aging.

2 Method

2.1 Experimental setup

Nine experiments (see Table 1) were carried out in the smog chamber of the Paul Scherrer Institute (PSI): a 27 m^3 Teflon bag suspended in a temperature-controlled wooden housing. Four xenon arc lamps (4 kW rated power, 1.55×10^5 lumens each, XBO 4000 W/HS, OSRAM) were used to simulate the solar light spectrum. In addition, during seven of the nine experiments 80 UV lights (Philips, Cleo performance 100 W) located underneath the SC bag were illuminated to accelerate the aging process. The smog chamber housing is covered inside with a reflecting aluminum foil to maintain light intensity and light diffusion. A comprehensive description of the PSI smog chamber is available in Paulsen et al. (2005).

2.1.1 Introduction of particle and gas phase reactants into the chamber

During all experiments, photooxidation of the biogenic precursor α-pinene in the presence of nitrogen oxides (NO_x) led to secondary aerosol formation and growth. Liquid phase α-pinene (98 %, Aldrich) and optionally the hydroxyl radical (OH) tracer (9-fold deuterated butanol, 98 %, D9, Cambridge Isotope Laboratories), hereafter referred to

ACPD
12, 24735–24764, 2012

as butanol-d9, were sequentially injected with a syringe into an evaporation glass bulb heated to 80 °C. The two gas phase compounds were carried with dilution and flush flows into the bag (each 15 l min^{-1}, maintained for 15 min) from an air purifier (737–250 series, AADCO Instruments, Inc., USA), further referred to as "pure air". The experiments were carried out at 40–50% relative humidity (RH), except experiment 7, where the prevailing RH was 28 ± 2 %. The temperature (T) varied within a range of 21 °C to 24 °C between experiments. Three NO_x sources (HONO, NO and NO_2) were added either in combination or separately during the different experiments. Table 1 provides an overview of the initial α-pinene concentrations, maximum wall loss corrected (wlc) organic mass concentrations, RH, initial NO_2 concentration before lights were switched on, average NO and NO_2 concentrations during the experiments, the radiation source(s) and the seed added.

HONO was used as a source of both NO and OH, except for experiments 5 and 6. It was produced by continuous ? mixing of sodium nitrite ($NaNO_2$, 1–3 mmol l^{-1}) and sulphuric acid (H_2SO_4, 10 mmol l^{-1}) solutions in a reaction vessel by means of a peristaltic pump (Taira and Kanda, 1990). The HONO product was entrained in 2.3–2.7 l min^{-1} pure air depending on the experiment. 1–5 ppbv (±10 %) of HONO was injected before lights on, to provide NO_x and enable photochemistry immediately after lights on (initial concentrations: see Supplement Table S1). The injection continued throughout the experiments to maintain a similar NO concentration level.

In experiments 5 and 6, NO_2 served as the NO_x source, with 6.9 ± 0.7 ppbv and 19.0 ± 1.9 ppbv NO_2 (purity: 98 %; 1005 ppmv ±3 %), respectively, injected before lights on. During experiment 4, NO (99.8 %; 1005 ppmv ±2 %) was continuously injected in addition to HONO and the flow was decreased stepwise from 10.0 to 3.8 ml min^{-1} (0.37 to 0.14 ppbv min^{-1}) which resulted in a slower increase of NO_2 and a leveling off of NO in the chamber.

Before switching on the lights during experiment 7, a suspension of 50 µl l^{-1} Tokai black printer ink containing black carbon and a solution of 4 g l^{-1} ammonium hydrogen sulfate (NH_4HSO_4), both in water, were sequentially nebulized and introduced into the

ACPD
12, 24735–24764, 2012

chamber with 0.6 l min^{-1} and a dilution flow of 10 l min^{-1} to act as seed particles. During experiments 3 and 4, 50 pptv SO_2 (99.98 %; 502 ppmv ± 2 %) was injected to photochemically produce H_2SO_4 nucleation, providing an aerosol surface rapidly and thus accelerate the SOA formation. In experiment 6, eight hours after lights on, 123 ± 4 ppbv of O_3 were added to the existing concentration of 41 ± 1 ppbv to investigate whether this would accelerate oxidation compared to the earlier period of the experiment. To minimize SOA formation by α-pinene ozonolysis, the injection was performed only after 99 % of the α-pinene had reacted.

Once all initial gas and aerosol phase components were present in the bag, a 20 to 30-min mixing period was allowed before the lights were switched on. After each experiment the smog chamber was cleaned by the injection of several ppmv of ozone for 5 h and irradiation for 10 h with UV lights at 20 °C, followed by a flushing period with pure air and high relative humidity (~ 70 %) at 30 °C for at least 20 h. To ensure that the organic matter (OM) formed during the experiments is not significantly influenced by background contamination in the smog chamber, blank experiments before, during and after the campaign were carried out. During two blank experiments at RH 50 % with neither HONO nor seed aerosol present, the maximum mass concentration was below 0.04 µg m^{-3} after 5 h and 8 h exposure to UV and xenon lights. A blank experiment with ammonium sulfate $(NH_4)_2SO_4$ seed, HONO and a relative humidity of 85 % yielded a peak organic mass concentration of 1.7 ± 0.1 µg m^{-3} 30 min after lights on. The two unseeded blank experiments without HONO possibly underestimate the organic mass yield due to the missing OH source, while the seeded blank experiment at 85 % RH possibly overestimate the blank by providing a large aqueous volume for organics to partition in. Thus, the different blank experiments represent lower and upper limits for contamination in the smog chamber. All experiments were carried at relative humidities ≦ 50 %. Experiment 7 (which is most similar to the seeded blank experiment) included a concentration of 69.2 µg m^{-3} and thus an organic mass concentration well above the blank value.

ACPD
12, 24735–24764, 2012

2.1.2 Instrumental setup

Various instruments were used to monitor gas and aerosol properties in the PSI smog chamber. A high resolution time-of-flight aerosol mass spectrometer (HR-ToF-AMS, Aerodyne Research, Inc., Billerica, MA, USA) was operated online to measure the chemical composition of non-refractory submicron particles (DeCarlo et al., 2006). Because this instrument samples at a low flow rate (0.1 l min^{-1}), a supporting flow of ~ 3 l min^{-1} was maintained parallel to the AMS inlet to minimize diffusive losses in the sampling lines. Gas phase compounds with a higher proton affinity than water (166.5 kcal mol^{-1}) were measured with a proton transfer reaction mass spectrometer (PTR-MS, Ionicon). Mass-to-charge ratios related to α-pinene (m/z 81 and m/z 137) and the OH tracer butanol-d9 (m/z 66) were analyzed in detail (see Sect. 2.2). A chemiluminescence-based NO_x instrument (Monitor Labs 9841A NO_x analyzer) was attached to the HONO source to monitor the injected concentration throughout the experiment. A modified NO_x instrument including a photolytic NO_2-to-NO converter (Thermo Environmental Instruments 42C trace level NO_x analyzer) and two ozone monitors (Monitor Labs 8810 ozone analyzer, Environics S300 ozone analyzer) monitored the gas phase in the chamber. A scanning mobility particle sizer (TSI: CPC 3022A, DMA long, classifier 3081) and a condensation particle counter (TSI CPC 3025A) measured the aerosol size distribution and the total particle number concentration ($d_{\text{mobility}} > 7$ nm), respectively.

2.2 OH exposure as comparison scale

Depending on the design of smog chamber experiments, the OH concentration and thus the photochemical age of the reaction system can vary considerably between experiments. Furthermore, within a single experiment the photochemical age is not necessarily directly proportional to the light exposure time. Therefore we here discuss reaction time in terms of OH exposure (unit: cm^{-3} h), defined as the OH concentration integrated over time. This scale is preferable when comparing the evolution of

ACPD
12, 24735–24764, 2012

experiments, especially when observing oxidation processes, as it is the chemically relevant aging time. In this study we determine OH exposures combining two methods: an OH tracer method introduced by Barmet et al. (2012) and a method based on the initial decay of the gas phase precursor α-pinene.

2.2.1 OH tracer method

1.5 µl (corresponding to ~ 14.5 ppbv) of the OH tracer butanol-d9 (detected as $M + H^+ - H_2O$ at *m/z* 66) was injected into the chamber via a heated glass bulb (Sect. 2.1.1). The OH tracer was present during the last hour of experiment 5, the second half of experiment 6, and for the entirety of experiments 3 and 4. Butanol-d9 is consumed by reaction with OH and diluted by the HONO input described in Sect. 2.1.1 (we assume as a first approximation a constant chamber volume, V) following the reaction kinetics governed by Eq. (1):

$$\frac{\mathrm{d(butanol\text{-}d9)}}{\mathrm{d}t} = -k_{\mathrm{OH,\ butanol\text{-}d9}} \cdot [\mathrm{OH}] \cdot [\mathrm{butanol\text{-}d9}] - \frac{f_{\mathrm{dil}}}{V} \cdot [\mathrm{butanol\text{-}d9}] \quad (1)$$

Where $k_{\mathrm{OH,\ butanol\text{-}d9}} = 3.4 \times 10^{-12}\ \mathrm{cm^3\ molecules^{-1}\ s^{-1}}$ and V = chamber volume (27 $\mathrm{m^3}$), f_{dil} = dilution flow ($\mathrm{m^3\ s^{-1}}$).

$$\text{OH exposure} = -\int_{t_1=0}^{t} \left(\frac{1}{k_{\mathrm{OH,\ butanol\text{-}d9}}} \cdot \left(\frac{\Delta \ln(\mathrm{butanol\text{-}d9})}{\Delta t} + \frac{f_{\mathrm{dil}}}{V} \right) \right) \mathrm{d}t \quad (2)$$

The slope of the temporal decay of ln(butanol-d9) at each time step was divided by the reaction rate constant $k_{\mathrm{OH,butanol\text{-}d9}}$ and corrected for the dilution to derive the OH concentration at each time step. Integrating this term with time Eq. (2) results in the OH exposure (Barmet et al., 2012). This method was used for the entirety of experiments 3 and 4.

ACPD
12, 24735–24764, 2012

2.2.2 α-pinene method

As well as the OH tracer decay, the decay of α-pinene can be utilized to derive the OH concentration. Compared to the OH tracer method, limitations of this method are the finite presence of α-pinene and its simultaneous reaction with both OH and O_3 as shown by Eq. (3). The OH exposure was therefore derived from the decay of ln(α-pinene), while correcting for the time-dependent reaction with O_3 and, if present, for the dilution of the chamber air due to the HONO input (described in Sect. 2.1.1) as shown in Eq. (4).

$$\frac{\mathrm{d}(\alpha\text{-pinene})}{\mathrm{d}t} = -k_{\mathrm{OH}} \cdot [\mathrm{OH}] \cdot [\alpha\text{-pinene}] - k_{\mathrm{O_3}} \cdot [\mathrm{O_3}] \cdot [\alpha\text{-pinene}] - \frac{f_{\mathrm{dil}}}{V} \cdot [\alpha\text{-pinene}], \quad (3)$$

where $k_{\mathrm{OH}} = 5.3 \times 10^{-11}\,\mathrm{cm^3\,molecules^{-1}\,s^{-1}}$ and $k_{\mathrm{O_3}} = 8.9 \times 10^{-17}\,\mathrm{cm^3\,molecules^{-1}\,s^{-1}}$,

$$\text{OH exposure} = -\int_{t_1=0}^{t} \left(\frac{1}{k_{\mathrm{OH}}} \cdot \left(\frac{\Delta \ln(\alpha\text{-pinene})}{\Delta t} + k_{\mathrm{O_3}} \cdot [\mathrm{O_3}] + \frac{f_{\mathrm{dil}}}{V} \right) \right) \mathrm{d}t \quad (4)$$

Only data fulfilling the criterion α-pinene ≥ 1 ppbv were used to ensure all measurements fall well above the PTR-MS detection limit. After α-pinene decayed below 1 ppbv, the OH concentration was assumed to be constant for the rest of the experiment time for experiments with continuous HONO addition.

2.2.3 Application of the methods to the dataset

For experiments 3 and 4, with both α-pinene and butanol-d9 present for the whole experiment time, a comparison of the two methods was performed (see Fig. S1 in the Supplement). The methods agree well for the later experiment time, which shows that the α-pinene method is valid at least for experiments with constant HONO input and thus a constant source of OH radicals.

ACPD
12, 24735–24764, 2012

The α-pinene method was utilized to derive the OH concentration of experiments 7, 8 and 9 with constant HONO input and α-pinene above detection limit for at least 1.3 h. The OH exposure from a repeat experiment using the butanol-d9 method was applied to experiments 1 and 2, conducted at substantial higher HONO/α-pinene ratios (0.2 and 0.4, respectively). The fast decay of α-pinene within the first 30 min during those two experiments due to the high accumulated HONO concentration before lights on and off-gassing from the walls after lights on, as previously measured by Metzger et al. (2008), gives rise to an overestimation of the OH exposure using the α-pinene method including the assumption of a constant OH concentration after the α-pinene is consumed. The repeat experiment shows the same characteristics in the α-pinene decay, but having the OH tracer butanol-d9 present for the whole experiment. A comparison of the three experiments is shown in Fig. S3 of the Supplement. In this way an overestimation of the OH concentration later in the experiment could be avoided.

In the course of experiments 5 and 6, the initially added NO_x concentration decayed to zero, which results in a substantial change in the gas phase chemistry including the production of ozone and thus OH. For the case of experiment 6, the ozone leveled off before being increased artificially by the addition of 123 ± 4 ppbv O_3 eight hours after lights on. For those two experiments, merged OH exposures derived from the α-pinene decay in the beginning and the decay of butanol added towards the end of the experiment were determined.

A compilation of the derived OH exposures is shown in Fig. S4 in the Supplement. When comparing experiments utilizing the α-pinene derived OH exposure, one has to keep in mind that the OH concentration is assumed to be constant after the drop below the threshold of 1 ppbv α-pinene. This extrapolation leads to uncertainties of the α-pinene derived OH exposure, which increases with experiment time. Nevertheless these uncertainties do not alter the main outcome of the study.

ACPD
12, 24735–24764, 2012

2.3 Wall loss correction

The measured aerosol mass concentration in the smog chamber is the net result of mass produced in the chamber and mass lost to the walls. In this study wall loss rates were determined from a period near the end of the experiment where chemical changes to the aerosol have slowed to the point that wall losses are expected to be the dominant factor controlling changes in the measured particle mass. The measured (AMS) aerosol mass during this period was fitted with an exponential. The data were then corrected by dividing the measured organic mass concentration by the exponential decay. Selecting a period when minor mass production is still possible leads to a lower limit for the wall loss correction assuming no major fragmentation due to the UV light exposure. This respective period can be identified by a constant resulting mass concentration in the end of the experiment. Figure S2 in the Supplement demonstrates the correction method for experiment 5.

3 Results

3.1 General reproducibility of the aerosol degree of oxygenation

The vaporization and ionization processes in the AMS fragment the sampled aerosol compounds. As described in the Introduction, the organic mass fraction f_{44} (defined as the organic signal at *m/z* 44 normalized to the total organic mass) is often related to carboxylic/organic acids and is proportional to the atomic O : C ratio whereas the organic mass fraction f_{43} is related to aldehydes, ketones and alcohols. The higher the f_{44}, the more oxygenated the aerosol. The f_{44}-f_{43} space was used to separate the two factors LV-OOA and SV-OOA (Ng et al., 2010) and is used in Fig. 1 to describe the chemical evolution of aerosol derived from α-pinene photooxidation in this study. The legend shows the final organic mass concentration for each experiment after wall loss correction. Despite varying organic mass concentrations, OH concentrations, NO_x

ACPD
12, 24735–24764, 2012

concentrations and RH in the smog chamber (see Table 1), all experiments are located within the same region on the right side of the triangle originating from average ambient data (Ng et al., 2010). During the on-going oxidation reactions in the smog chamber more highly oxygenated products are formed, resulting in an increased f_{44} together with a decreased f_{43}. This process leads to a pathway in Fig. 1 from the lower right to the upper left. For the first time, an organic mass fraction f_{44} as high as many ambient LV-OOA and well above the SV-OOA range is obtained from an α-pinene photooxidation smog chamber study at ambient-like OH concentrations. Together with e.g. SOA from wood burning found on the left hand side (Heringa et al., 2011), the mixture of aerosol from several sources can explain a wide range of the empirically derived triangle.

3.2 Dependence of degree of oxygenation on the organic mass concentration

Figure 2 shows the evolution of organic mass fraction f_{44} as a function of organic mass fraction f_{43}, both averaged over 30 min intervals, for three selected experiments (Expt. No. 3, 4, 6), during which the OH tracer butanol-d9 was present in the chamber for most of the experiment. The respective OH exposures were derived according to the methods described in Sect. 2.2. The data is terminated at an OH exposure of 3.5×10^7 cm^{-3} h for all three experiments to allow for a comparison of f_{44} and f_{43} depending only on the organic mass concentration. The organic mass concentrations (averages and standard deviation for ±15 min) at this OH exposure in experiments 6, 3 and 4 were $38.7 \pm 0.5\,\mu g\,m^{-3}$, $6.2 \pm 0.1\,\mu g\,m^{-3}$ and $1.4 \pm 0.1\,\mu g\,m^{-3}$, respectively. The corresponding averaged f_{44} values, reported here as percentage, were 11.9 ± 0.1 %, 14.1 ± 0.4 % and 15.9 ± 1.3 %, respectively. The data clearly show that at the same OH exposure, the degree of oxygenation is dependent on the total organic mass concentration present in the chamber.

For a comprehensive comparison of all experiments described in this study, the OH exposure was utilized as the aging scale. The evolution of f_{44} as a function of organic mass concentration is shown in Fig. 3, with each of the nine experiments marked by a different symbol and color-coded by the OH exposure. Initially, there is a period of

ACPD
12, 24735–24764, 2012

rapid mass increase with a slow increase in f_{44}, followed by a later period of a continuous f_{44} increase with only a slight further increase in mass. The initial period is likely governed by condensation of early-generation, semi-volatile products and their condensation therefore yields a lower increase in f_{44}. As aging proceeds, the gas phase organics become more oxidized. Their condensed-phase products are similarly more oxygenated (higher f_{44}). Additional aging of the particles is possible through the repartitioning of semi-volatile condensed-phase OA to the gas phase, followed by gas phase oxidation and re-condensation of the oxygenated products. This process also increases f_{44} while only slightly affecting the total OA mass. Nevertheless, the significantly varying mass concentrations between the nine experiments are more important than the slight mass increase within one experiment when it comes to partitioning effects. The more organic mass concentration available in the chamber for volatile organic compounds to condense on, the more semi-volatile compounds besides the low-volatility compounds can be transferred to the aerosol phase (Donahue et al., 2006). As shown by Ng et al. (2010), more oxygenated compounds tend to be less volatile. At low mass concentrations, the less oxygenated semi-volatile species are less likely to partition to the particle phase. Their reaction with OH proceeds in the gas phase until either (1) they become sufficiently oxygenated to condense (which requires a higher level of oxygenation than at high mass concentrations) or (2) they fragment sufficiently that they will never enter the particle phase. Either way, the net O : C ($\sim f_{44}$) ratio of the low concentration experiments is higher.

In Fig. 3, the color-coded squares correspond to OH exposures of 2, 4, 6, 8 and 11×10^7 cm^{-3} h, respectively, for which the organic mass fraction f_{44} and the organic mass concentration (wlc) were averaged (±15 min). Experiments with similar organic mass concentrations are grouped in Fig. 3 as follows: low concentration experiments: 1, 4; medium conc.: 2, 3, 5; high conc.: 6, 7, 8, 9. Average group values were calculated for those groups where the OH exposure reached the threshold value during at least one experiment. Table 2 presents the corresponding values of organic mass fraction f_{44} and organic mass concentration (wlc) for the five different OH exposures.

ACPD
12, 24735–24764, 2012

For visualization, these group mean values at OH exposures of 2 and 4×10^7 cm^{-3} h are represented by black filled squares and connected with a line in Fig. 3. The significant dependence of f_{44} on the organic mass (note the logarithmic scale of the x-axis) is approximated by the slope $\Delta f_{44}/\Delta$org (wlc) between low and medium organic mass concentrations and between medium and high organic mass concentrations and summarized in Table 3. The slope is steeper for the lower organic mass range than for the higher mass range. This implies that at typical atmospheric concentration levels ($\sim$ 1–30 µg m^{-3}), partitioning effects on SOA oxygenation are even more sensitive to the organic mass concentration than for the higher-than-atmospheric concentrations used in most previous smog chamber studies. Using typical atmospheric organic mass concentrations in smog chamber studies is not only crucial to reproduce the volatility and degree of oxygenation of ambient SOA, but also to accurately determine cloud condensation nuclei activity due to the dependence of the hygroscopicity on f_{44} ($\sim$O : C ratio).

3.3 Dependence of degree of oxygenation on the OH exposure

The degree of oxygenation reached by α-pinene SOA depends on both the organic mass concentration (discussed above) and the OH exposure. For each experiment, the slope of $\Delta f_{44}/\Delta$(OH exposure) was fitted for the part of the experiment dominated by aging (rather than mass production), defined as the period after the peak of suspended organic mass concentration was reached in the chamber. The individual slopes are shown in Fig. S6 and summarized in Table S2 in the Supplement. On average, an OH exposure of $2.9 \pm 1.3 \times 10^7$ cm^{-3} h is needed to increase f_{44} by 1 %. Table 4 shows OH exposures (and corresponding organic mass concentrations (wlc)) required to obtain $f_{44} > 15$ %, a representative value for LV-OOA, for the four experiments where this threshold was exceeded. For experiments where the threshold of 15 % f_{44} was not reached, the derived slopes of $\Delta f_{44}/\Delta$(OH exposure) and the value pair (f_{44}/OH exposure) at peak suspended organic mass were utilized to estimate the total OH exposure

ACPD
12, 24735–24764, 2012

needed to do so. The OH exposure observed for oxidation of SOA to mostly LV-OOA in the Mexico City plume (~ 4–5×10^7 cm^{-3} h, six hours air transport time) as estimated from aircraft measurements (DeCarlo et al., 2010; Dusanter et al., 2009) is within the range of OH exposures required in this study, despite different precursors.

3.4 Classification of chemical composition using reference mass spectra

To classify the aerosol chemical composition found in this study with respect to ambient data, the SC organic mass spectra were compared to reference mass spectra retrieved from ambient measurements. These reference spectra were derived with PMF analysis of a number of ambient datasets and compiled by Ng et al. (2011) and are available on the AMS Spectral Database (Ulbrich et al., 2009). Figure 4 shows R^2 values (Pearson correlation) of the LV-OOA (filled circles) and SV-OOA (empty circles) unit mass spectra from (Ng et al., 2011) with unit mass spectra from this study as a function of wall loss corrected organic mass concentration. The mass spectra for each of the nine experiments were averaged for 30 min surrounding the OH exposures of 2×10^7 cm^{-3} h and 4×10^7 cm^{-3} h, respectively (i.e. the selected exposure ±15 min). To prevent an artificial bias in the correlation test, data from all organic mass-to-charge ratios assumed directly proportional to *m/z* 44, namely *m/z* 16, 17, 18, 19, 20 and 28, were excluded from the correlation test. The general trend for both exposures shows increased correlation with LV-OOA and decreased correlation with SV-OOA with decreasing mass concentration, when comparing data between the three groups introduced in Sect. 3.1. For all mass concentrations, an increasing R^2 (LV-OOA) and a decreasing R^2 (SV-OOA) with increasing OH exposure is found. The dependence on mass concentration occurs for the partitioning-related reasons discussed above in conjunction with increased O : C for low mass concentrations, while the dependence on OH exposure occurs because SOA spectra become more LV-OOA-like with photochemical age. For the high concentration experiments, the difference between R^2 (SV-OOA) and R^2 (LV-OOA) is more pronounced for the lower OH exposure than for the higher OH exposure. Nevertheless, the lower R^2 (LV-OOA) of the high concentration experiments compared to the low

ACPD
12, 24735–24764, 2012

concentration experiments even for the enhanced OH exposure suggest a substantial difference in the chemical composition as a function of the organic aerosol loading. The low concentration experiments (organic mass $< 15\,\mu g\,m^{-3}$ in Fig. 4) correlate strongly with LV-OOA ($R^2 > 0.9$) for an OH exposure of $4 \times 10^7\,cm^{-3}\,h$. This indicates that for low organic mass concentrations, SOA from smog chamber α-pinene photooxidation yields LV-OOA-like mass spectra after a sufficient oxidation time. Also for higher OH exposures, the correlation to LV-OOA is higher than 89 % for the low concentration experiments, while the R^2 values with SV-OOA decrease dramatically (Fig. S5 in the Supplement).

4 Conclusions

A series of smog chamber experiments were conducted to identify driving factors responsible for the discrepancy between ambient and smog chamber aerosol degree of oxygenation, which in turn strongly affects aerosol volatility and hygroscopicity. In this study, the aerosol products from α-pinene photooxidation are located within the f_{44}-f_{43}-space bounding the range of PMF factors previously identified in ambient SOA (Ng et al., 2010). The organic mass fraction f_{44}, a proxy for the degree of oxygenation, is higher for low organic mass loadings and its dependence on organic mass concentrations is even more pronounced in the range of typical atmospheric mass concentrations. This has been shown in a comparison of nine smog chamber experiments where the OH exposure was estimated to isolate the effects of mass loading and photochemical age. We conclude that low (near-ambient level) organic mass loading is required in order to obtain oxygenation levels comparable to those of the low-volatility oxygenated organic aerosol (LV-OOA) PMF factors retrieved in numerous field campaigns. On average, an OH exposure of $2.9 \pm 1.3 \times 10^7\,cm^{-3}\,h$ is needed to increase f_{44} by 1 % during aerosol aging. This study marks the first smog chamber production of LV-OOA-like SOA from the atmospherically relevant precursor α-pinene. For ozonolysis of α-pinene, the degree of oxygenation falls in the range of SV-OOA even at low

ACPD
12, 24735–24764, 2012

concentrations (Shilling et al., 2009; Ng et al., 2010). This is in line with the hypothesis of Donahue et al. (2012) that further aging occurs with OH after/together with ozonolysis. A correlation test between measured SOA and reference LV-OOA (Ng et al., 2011) aerosol mass spectra shows Pearson's R^2 values larger than 90 % for a sufficient OH exposure in the chamber in low mass concentration experiments ($\sim$ 1.5–15 µg m^{-3}). To accurately simulate the chemical properties, volatility and hygroscopicity of ambient aerosol, smog chamber studies must not only be performed at reasonable oxidant concentrations, but also at near-ambient mass concentrations.

Supplementary material related to this article is available online at: http://www.atmos-chem-phys-discuss.net/12/24735/2012/acpd-12-24735-2012-supplement.pdf.

Acknowledgements. This work has been supported by the EU 7th Framework projects EUROCHAMP-2 and PEGASOS, as well as the Swiss National Science Foundation. We thank Rene Richter and Günther Wehrle for their technical support at the smog chamber, and in addition Stephen Platt and Robert Wolf for their support during the experiments.

References

Aiken, A. C., DeCarlo, P. F., Kroll, J. H., Worsnop, D. R., Huffman, J. A., Docherty, K. S., Ulbrich, I. M., Mohr, C., Kimmel, J. R., Sueper, D., Sun, Y., Zhang, Q., Trimborn, A., Northway, M., Ziemann, P. J., Canagaratna, M. R., Onasch, T. B., Alfarra, M. R., Prévôt, A. S. H., Dommen, J., Duplissy, J., Metzger, A., Baltensperger, U., and Jimenez, J. L.: O/C and OM/OC ratios of primary, secondary, and ambient organic aerosols with high-resolution time-of-flight aerosol mass spectrometry, Environ. Sci. Technol., 42, 4478–4485, 2008.

Barmet, P., Dommen, J., DeCarlo, P. F., Tritscher, T., Praplan, A. P., Platt, S. M., Prévôt, A. S. H., Donahue, N. M., and Baltensperger, U.: OH clock determination by proton transfer reaction mass spectrometry at an environmental chamber, Atmos. Meas. Tech., 5, 647–656, doi:10.5194/amt-5-647-2012, 2012.

ACPD
12, 24735–24764, 2012

Chhabra, P. S., Ng, N. L., Canagaratna, M. R., Corrigan, A. L., Russell, L. M., Worsnop, D. R., Flagan, R. C., and Seinfeld, J. H.: Elemental composition and oxidation of chamber organic aerosol, Atmos. Chem. Phys., 11, 8827–8845, doi:10.5194/acp-11-8827-2011, 2011.

DeCarlo, P. F., Kimmel, J. R., Trimborn, A., Northway, M. J., Jayne, J. T., Aiken, A. C., Gonin, M., Fuhrer, K., Horvath, T., Docherty, K. S., Worsnop, D. R., and Jimenez, J. L.: Field-deployable, high-resolution, time-of-flight aerosol mass spectrometer, Anal. Chem., 78, 8281–8289, 2006.

DeCarlo, P. F., Ulbrich, I. M., Crounse, J., de Foy, B., Dunlea, E. J., Aiken, A. C., Knapp, D., Weinheimer, A. J., Campos, T., Wennberg, P. O., and Jimenez, J. L.: Investigation of the sources and processing of organic aerosol over the Central Mexican Plateau from aircraft measurements during MILAGRO, Atmos. Chem. Phys., 10, 5257–5280, doi:10.5194/acp-10-5257-2010, 2010.

Donahue, N. M., Robinson, A. L., Stanier, C. O., and Pandis, S. N.: Coupled partitioning, dilution, and chemical aging of semivolatile organics, Environ. Sci. Technol., 40, 2635–2643, 2006.

Donahue, N. M., Henry, K. M., Mentel, T. F., Kiendler-Scharr, A., Spindler, C., Bohn, B., Brauers, T., Dorn, H. P., Fuchs, H., Tillmann, R., Wahner, A., Saathoff, H., Naumann, K.-H., Moehler, O., Leisner, T., Mueller, L., Reinnig, M.-C., Hoffmann, T., Salo, K., Hallquist, M., Frosch, M., Bilde, M., Tritscher, T., Barmet, P., Praplan, A. P., DeCarlo, P. F., Dommen, J., Prévôt, A. S. H., and Baltensperger, U.: Aging of secondary organic aerosol: connecting chambers to the atmosphere, Proc. Natl. Acad. Sci. USA, in press, 2012.

Duplissy, J., Gysel, M., Alfarra, M. R., Dommen, J., Metzger, A., Prévôt, A. S. H., Weingartner, E., Laaksonen, A., Raatikainen, T., Good, N., Turner, S. F., McFiggans, G., and Baltensperger, U.: Cloud forming potential of secondary organic aerosol under near atmospheric conditions, Geophys. Res. Lett., 35, L03818, doi:10.1029/2007GL031075, 2008.

Duplissy, J., DeCarlo, P. F., Dommen, J., Alfarra, M. R., Metzger, A., Barmpadimos, I., Prévôt, A. S. H., Weingartner, E., Tritscher, T., Gysel, M., Aiken, A. C., Jimenez, J. L., Canagaratna, M. R., Worsnop, D. R., Collins, D. R., Tomlinson, J., and Baltensperger, U.: Relating hygroscopicity and composition of organic aerosol particulate matter, Atmos. Chem. Phys., 11, 1155–1165, doi:10.5194/acp-11-1155-2011, 2011.

Dusanter, S., Vimal, D., Stevens, P. S., Volkamer, R., and Molina, L. T.: Measurements of OH and HO_2 concentrations during the MCMA-2006 field campaign – Part 1: Deployment of the

ACPD
12, 24735–24764, 2012

Indiana University laser-induced fluorescence instrument, Atmos. Chem. Phys., 9, 1665–1685, doi:10.5194/acp-9-1665-2009, 2009.
Heringa, M. F., DeCarlo, P. F., Chirico, R., Tritscher, T., Dommen, J., Weingartner, E., Richter, R., Wehrle, G., Prévôt, A. S. H., and Baltensperger, U.: Investigations of primary and secondary particulate matter of different wood combustion appliances with a high-resolution time-of-flight aerosol mass spectrometer, Atmos. Chem. Phys., 11, 5945–5957, doi:10.5194/acp-11-5945-2011, 2011.
Hodzic, A., Jimenez, J. L., Madronich, S., Canagaratna, M. R., DeCarlo, P. F., Kleinman, L., and Fast, J.: Modeling organic aerosols in a megacity: potential contribution of semi-volatile and intermediate volatility primary organic compounds to secondary organic aerosol formation, Atmos. Chem. Phys., 10, 5491–5514, doi:10.5194/acp-10-5491-2010, 2010.
Huffman, J. A., Docherty, K. S., Mohr, C., Cubison, M. J., Ulbrich, I. M., Ziemann, P. J., Onasch, T. B., and Jimenez, J. L.: Chemically-resolved volatility measurements of organic aerosol from different sources, Environ. Sci. Technol., 43, 5351–5357, 2009.
Jimenez, J. L., Canagaratna, M. R., Donahue, N. M., Prévôt, A. S. H., Zhang, Q., Kroll, J. H., DeCarlo, P. F., Allan, J. D., Coe, H., Ng, N. L., Aiken, A. C., Docherty, K. S., Ulbrich, I. M., Grieshop, A. P., Robinson, A. L., Duplissy, J., Smith, J. D., Wilson, K. R., Lanz, V. A., Hueglin, C., Sun, Y. L., Tian, J., Laaksonen, A., Raatikainen, T., Rautiainen, J., Vaattovaara, P., Ehn, M., Kulmala, M., Tomlinson, J. M., Collins, D. R., Cubison, M. J., E, Dunlea, J., Huffman, J. A., Onasch, T. B., Alfarra, M. R., Williams, P. I., Bower, K., Kondo, Y., Schneider, J., Drewnick, F., Borrmann, S., Weimer, S., Demerjian, K., Salcedo, D., Cottrell, L., Griffin, R., Takami, A., Miyoshi, T., Hatakeyama, S., Shimono, A., Sun, J. Y., Zhang, Y. M., Dzepina, K., Kimmel, J. R., Sueper, D., Jayne, J. T., Herndon, S. C., Trimborn, A. M., Williams, L. R., Wood, E. C., Middlebrook, A. M., Kolb, C. E., Baltensperger, U., and Worsnop, D. R.: Evolution of organic aerosols in the atmosphere, Science, 326, 1525–1529, doi:10.1126/science.1180353, 2009.
Lambe, A. T., Onasch, T. B., Massoli, P., Croasdale, D. R., Wright, J. P., Ahern, A. T., Williams, L. R., Worsnop, D. R., Brune, W. H., and Davidovits, P.: Laboratory studies of the chemical composition and cloud condensation nuclei (CCN) activity of secondary organic aerosol (SOA) and oxidized primary organic aerosol (OPOA), Atmos. Chem. Phys., 11, 8913–8928, doi:10.5194/acp-11-8913-2011, 2011.
Lanz, V. A., Alfarra, M. R., Baltensperger, U., Buchmann, B., Hueglin, C., and Prévôt, A. S. H.: Source apportionment of submicron organic aerosols at an urban site by factor analytical

ACPD
12, 24735–24764, 2012

modelling of aerosol mass spectra, Atmos. Chem. Phys., 7, 1503–1522, doi:10.5194/acp-7-1503-2007, 2007.

Lanz, V. A., Prévôt, A. S. H., Alfarra, M. R., Weimer, S., Mohr, C., DeCarlo, P. F., Gianini, M. F. D., Hueglin, C., Schneider, J., Favez, O., D'Anna, B., George, C., and Baltensperger, U.: Characterization of aerosol chemical composition with aerosol mass spectrometry in Central Europe: an overview, Atmos. Chem. Phys., 10, 10453–10471, doi:10.5194/acp-10-10453-2010, 2010.

Massoli, P., Lambe, A. T., Ahern, A. T., Williams, L. R., Ehn, M., Mikkilä, J., Canagaratna, M. R., Brune, W. H., Onasch, T. B., Jayne, J. T., Petäjä, T., Kulmala, M., Laaksonen, A., Kolb, C. E., Davidovits, P., and Worsnop, D. R.: Relationship between aerosol oxidation level and hygroscopic properties of laboratory generated secondary organic aerosol (SOA) particles, Geophys. Res. Lett., 37, L24801, doi:10.1029/2010GL045258, 2010.

Metzger, A., Dommen, J., Gaeggeler, K., Duplissy, J., Prévôt, A. S. H., Kleffmann, J., Elshorbany, Y., Wisthaler, A., and Baltensperger, U.: Evaluation of 1,3,5 trimethylbenzene degradation in the detailed tropospheric chemistry mechanism, MCMv3.1, using environmental chamber data, Atmos. Chem. Phys., 8, 6453–6468, doi:10.5194/acp-8-6453-2008, 2008.

Ng, N. L., Canagaratna, M. R., Zhang, Q., Jimenez, J. L., Tian, J., Ulbrich, I. M., Kroll, J. H., Docherty, K. S., Chhabra, P. S., Bahreini, R., Murphy, S. M., Seinfeld, J. H., Hildebrandt, L., Donahue, N. M., DeCarlo, P. F., Lanz, V. A., Prévôt, A. S. H., Dinar, E., Rudich, Y., and Worsnop, D. R.: Organic aerosol components observed in Northern Hemispheric datasets from Aerosol Mass Spectrometry, Atmos. Chem. Phys., 10, 4625–4641, doi:10.5194/acp-10-4625-2010, 2010.

Ng, N. L., Canagaratna, M. R., Jimenez, J. L., Chhabra, P. S., Seinfeld, J. H., and Worsnop, D. R.: Changes in organic aerosol composition with aging inferred from aerosol mass spectra, Atmos. Chem. Phys., 11, 6465–6474, doi:10.5194/acp-11-6465-2011, 2011.

Paulsen, D., Dommen, J., Kalberer, M., Prévôt, A. S. H., Richter, R., Sax, M., Steinbacher, M., Weingartner, E., and Baltensperger, U.: Secondary organic aerosol formation by irradiation of 1,3,5-trimethylbenzene-NO_x-H_2O in a new reaction chamber for atmospheric chemistry and physics, Environ. Sci. Technol., 39, 2668–2678, 2005.

Prinn, R. G., Huang, J., Weiss, R. F., Cunnold, D. M., Fraser, P. J., Simmonds, P. G., McCulloch, A., Harth, C., Salameh, P., O'Doherty, S., Wang, R. H. J., Porter, L., and Miller, B. R.:

ACPD
12, 24735–24764, 2012

Evidence for substantial variations of atmospheric hydroxyl radicals in the past two decades, Science, 292, 1882–1888, doi:10.1126/science.1058673, 2001.

Robinson, A. L., Donahue, N. M., Shrivastava, M. K., Weitkamp, E. A., Sage, A. M., Grieshop, A. P., Lane, T. E., Pierce, J. R., and Pandis, S. N.: Rethinking organic aerosols: semivolatile emissions and photochemical aging, Science, 315, 1259–1262, 2007.

Shilling, J. E., Chen, Q., King, S. M., Rosenoern, T., Kroll, J. H., Worsnop, D. R., DeCarlo, P. F., Aiken, A. C., Sueper, D., Jimenez, J. L., and Martin, S. T.: Loading-dependent elemental composition of α-pinene SOA particles, Atmos. Chem. Phys., 9, 771–782, doi:10.5194/acp-9-771-2009, 2009.

Slowik, J. G., Wong, J. P. S., and Abbatt, J. P. D.: Real-time, controlled OH-initiated oxidation of biogenic secondary organic aerosol, Atmos. Chem. Phys. Discuss., 12, 8183–8224, doi:10.5194/acpd-12-8183-2012, 2012.

Taira, M. and Kanda, Y.: Continuous generation system for low-concentration gaseous nitrous acid, Anal. Chem., 62, 630–633, 1990.

Ulbrich, I. M., Canagaratna, M. R., Zhang, Q., Worsnop, D. R., and Jimenez, J. L.: Interpretation of organic components from Positive Matrix Factorization of aerosol mass spectrometric data, Atmos. Chem. Phys., 9, 2891–2918, doi:10.5194/acp-9-2891-2009, 2009.

Volkamer, R., Jimenez, J. L., San Martini, F., Dzepina, K., Zhang, Q., Salcedo, D., Molina, L. T., Worsnop, D. R., and Molina, M. J.: Secondary organic aerosol formation from anthropogenic air pollution: rapid and higher than expected, Geophys. Res. Lett., 33, L17811, doi:10.1029/2006GL026899, 2006.

ACPD

12, 24735–24764, 2012

Table 1. Overview of experiment conditions. During experiments 5 and 6, the initially added NO_2 concentration decayed to zero in the course of the experiments. Org max (wlc) is the wall loss corrected organic mass concentration at the end of the experiment. Radiation sources are UV or xenon (xen) lights. The OH tracer butanol-d9 is abbreviated with but-d9. Black carbon (BC) and NH_4HSO_4 represent seed aerosol in experiment 7.

Expt. No.	Initial α-pinene ppb	Org max (wlc) $\mu g\,m^{-3}$	RH av(sd) %	NO av(sd) ppb	NO_2 av(sd)* ppb	Radiation source(s)	Added			
1	7	2.0	50(1)	3.9(0.6)	4.9(1.8)	UV+xen	HONO			
2	14	14.4	48(2)	3.0(0.4)	5.9(0.9)	UV+xen	HONO			
3	20	6.6	40(2)	0.3(0.1)	0.8(0.3)	UV+xen	HONO	but-d9	SO_2	
4	22	1.4	44(1)	4.2(0.9)	20.0(9.9)	UV+xen	HONO	but-d9	SO_2	NO
5	23	8.8	47(2)	0.6(0.9)	6.9(0.3)*	UV+xen		but-d9		
6	44	39.5	44(2)	0.3(0.8)	19.0(0.4)*	xen		but-d9		
7	45	69.2	28(2)	1.0(0.2)	3.6(1.3)	UV+xen	HONO	BC & NH_4HSO_4		
8	46	72.4	49(1)	2.0(1.1)	22.0(12.0)	xen	HONO			
9	50	79.1	47(1)	1.8(0.3)	9.0(3.0)	UV+xen	HONO			

* Initial NO_2 addition that decayed to zero during experiments 5 and 6.

ACPD
12, 24735–24764, 2012

Table 2. Group mean values of 30-min-averages of organic mass fraction f_{44} and wall loss corrected organic mass concentration, Org (wlc), for the three different groups (low/medium/high organic mass concentration) at given OH exposures.

		OH exposure (10^7 cm^{-3} h)				
		2	4	6	8	11
f_{44}	Low org mass	0.15	0.16	0.17	0.19*	0.20*
	Medium org mass	0.14	0.15	0.15	0.16	0.18*
	High org mass	0.11	0.12	0.13*		
Org (wlc) (µg m^{-3})	Low org mass	0.91	1.66	1.63	1.90*	1.89*
	Medium org mass	7.92	10.14	10.01	10.07	14.15*
	High org mass	57.16	72.11	76.45*		

* Data is not group mean, contains 30-min-averages of one experiment only.

ACPD
12, 24735–24764, 2012

Table 3. Slopes $\Delta f_{44}/\Delta$org (wlc) between group "low" and "medium" organic mass concentration and between "medium" and "high" organic mass concentration. "Low", "medium" and "high" mass concentrations are defined in Fig. 3 and the accompanying text.

		OH exposure (10^7 cm^{-3} h)	
	Org mass conc.	2	4
$\Delta f_{44}/\Delta$org (wlc) ($\%\,m^3\,\mu g^{-1}$)	low → medium	−0.13	−0.18
	medium → high	−0.05	−0.05

ACPD
12, 24735–24764, 2012

Table 4. The OH exposure needed to increase f_{44} above 15 % at the corresponding organic mass concentration (wlc). Values are measured for experiments 1, 2, 3 and 4 and estimated for experiments which don not exceed the threshold. The asterisk indicates the extrapolated OH exposure and the final measured organic mass concentration (wlc).

Expt. No.	OH exposure 10^7 cm^{-3} h	Org wlc µg m^{-3}
1	2.3	1.1
4	3.2	1.4
5	3.7*	8.8*
2	4.0	14.2
3	6.7	6.1
7	8.7*	69.2*
6	9.0*	39.5*
9	11.6*	79.1*
8	24.6*	72.4*

ACPD
12, 24735–24764, 2012

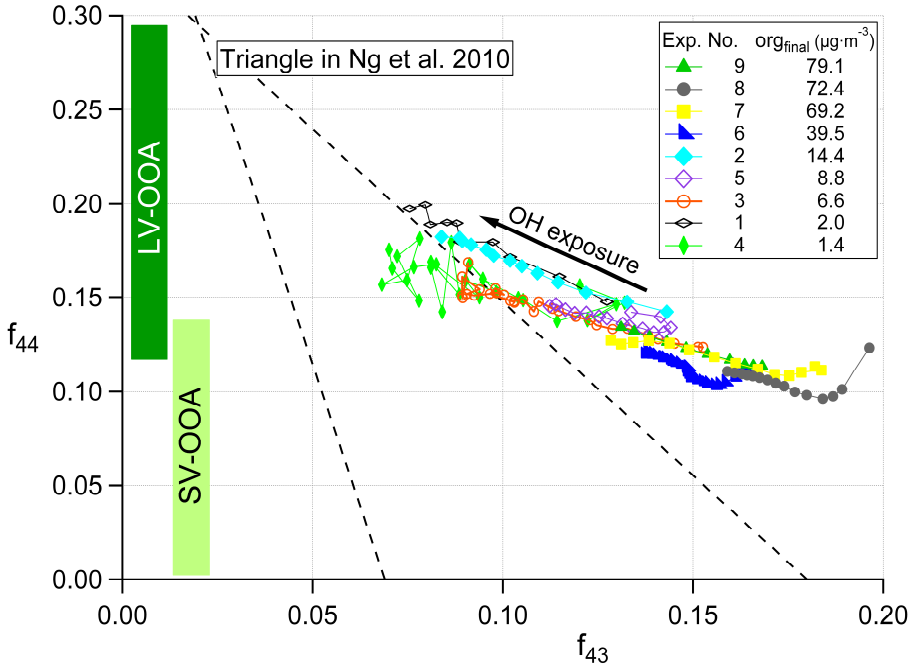

Fig. 1. 30-min averages of organic mass fraction f_{44} vs. organic mass fraction f_{43}. The legend shows the final wall loss corrected organic mass concentration in μg m^{-3} at the end of each experiment. Dashed lines represent the observed range of ambient SOA (Ng et al., 2010).

ACPD
12, 24735–24764, 2012

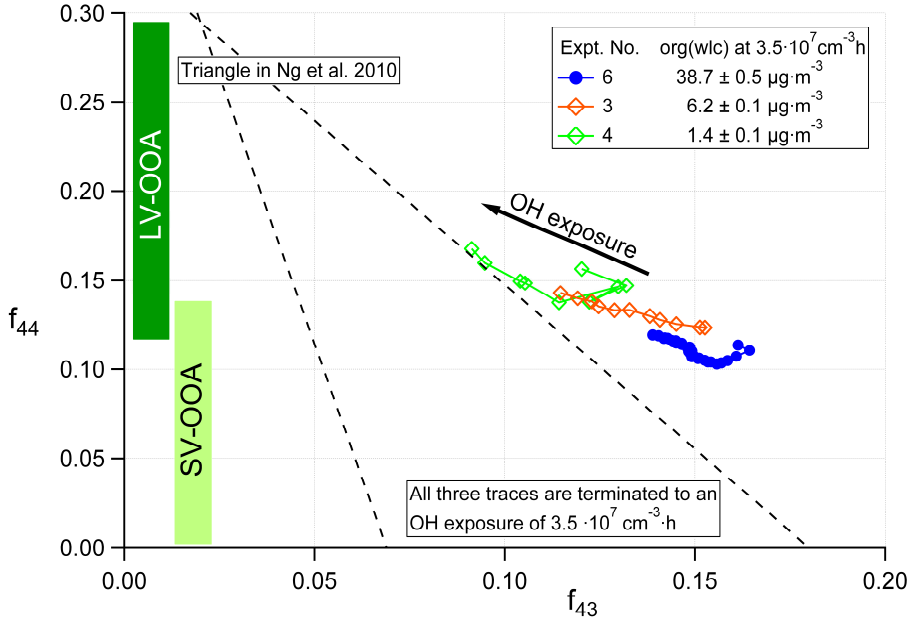

Fig. 2. Organic mass fraction f_{44} plotted against organic mass fraction f_{43} for three experiments with different organic mass loadings. Each data point represents a 30-min average. All traces terminate at the same OH exposure of 3.5×10^7 cm^{-3} h.

ACPD
12, 24735–24764, 2012

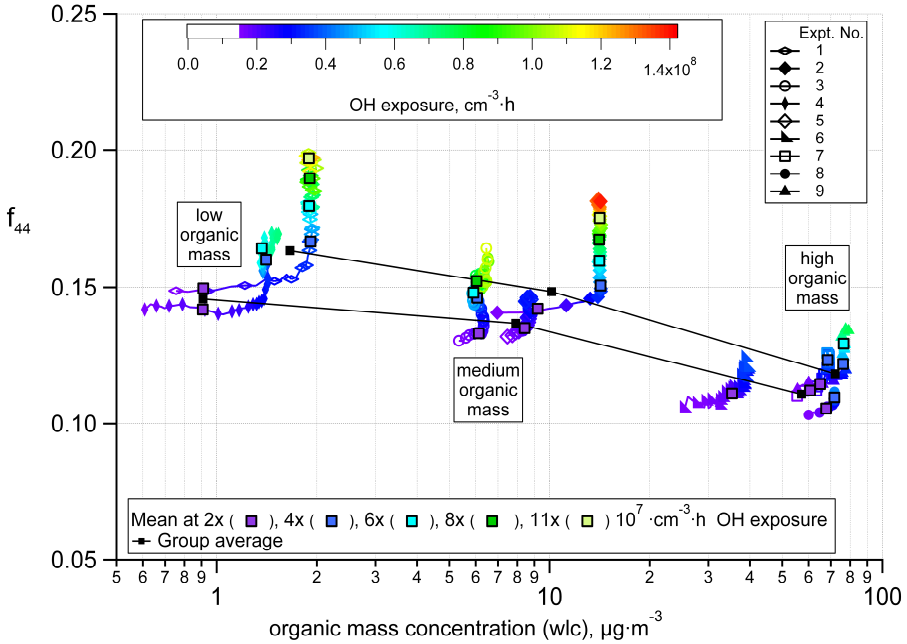

Fig. 3. Organic mass fraction f_{44} as a function of the organic mass concentration ($\mu g m^{-3}$) in the chamber. The color code indicates the OH exposure. 30-min mean values at selected OH exposures are represented by colored squares. The averages of these means for each "group" are represented by black filled squares and connected with a line.

ACPD
12, 24735–24764, 2012

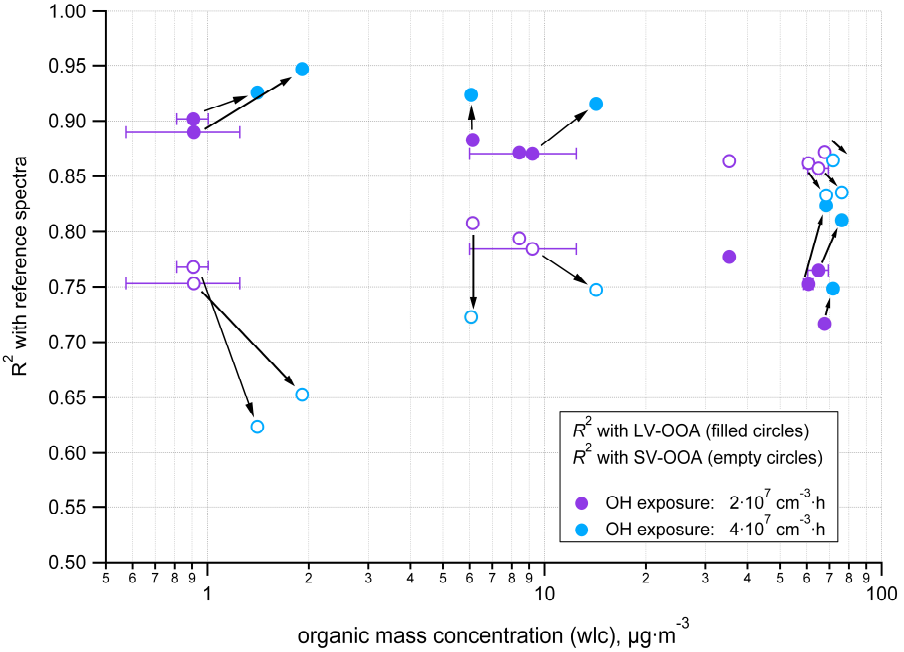

Fig. 4. Squares of the Pearson correlation coefficients, R^2, of measured mass spectra in comparison with LV-OOA (filled circles) and SV-OOA (empty circles) reference spectra (Ng et al., 2011) as a function of the organic mass concentration (wlc). The color code represents the OH exposure at the midpoint of a 30 min mass spectral average.

ACPD
12, 24735–24764, 2012